Michigan State University

National Superconducting Cyclotron Laboratory

PERCOLATION WITH BUBBLES AND TOROIDS

L. PHAIR, W. BAUER, and C.K. GELBKE

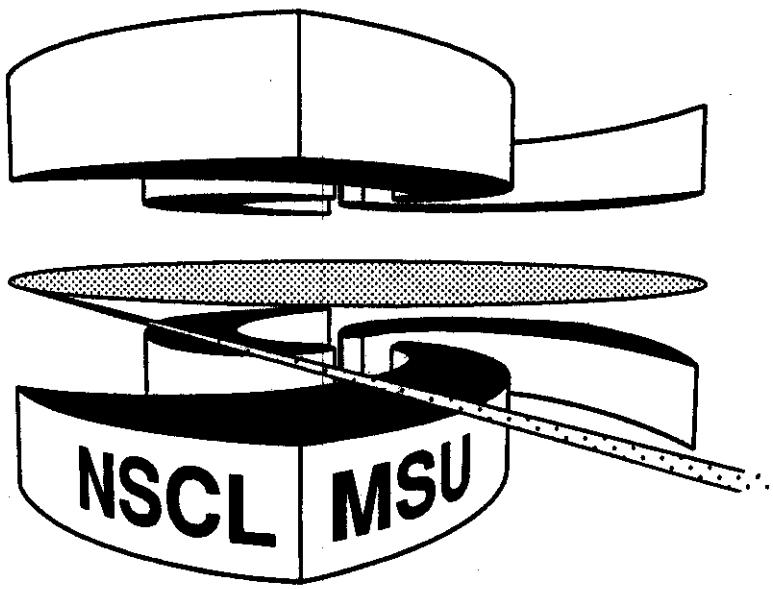

MSUCL-890 **APRIL 1993**

MSUCL-890
April, 1993

Percolation with Bubbles and Toroids

L. Phair, W. Bauer, and C.K. Gelbke

National Superconducting Cyclotron Laboratory
and
Department of Physics and Astronomy
Michigan State University
East Lansing, MI 48824, USA

Abstract:

Multifragment disintegration of finite systems with toroidal and bubble-shaped configurations is studied within the framework of a bond-percolation model. Calculations for these finite systems predict enhanced fragment production for less compact decay configurations. Power law fits to the predicted mass distributions reveal a strong sensitivity of the extracted critical exponents on the geometry of the decaying system.

The copious production of intermediate mass fragments (IMF: $3 \leq Z \leq 20$) in intermediate-energy heavy-ion collisions and its possible relation to a liquid-gas phase transition in nuclear matter is a subject of great current interest [1-5]. While current microscopic models fail to reproduce the observed large IMF multiplicities [6], significant insight has been gleaned from statistical treatments of fragment production [5-21]. Percolation models have been particularly useful [15-21] because they exhibit a well-defined phase transition for infinite systems and allow a straightforward assessment of finite-size effects [17,21]. They have been rather successful [15-17] in describing the observed [2] power-law behavior of measured fragment mass distributions, and in developing techniques to extract critical exponents [18] and test for critical behavior via scaling law approaches originally derived for infinite systems. A recent investigation [20] of fragment admixtures predicted by the standard bond-percolation model found rather good agreement with fragment admixtures measured for $^{36}Ar + ^{197}Au$ collisions; larger fragment admixtures measured for $^{129}Xe + ^{197}Au$ collisions, on the other hand, were found to be inconsistent with the model. In previous bond-percolation calculations, the disintegrating systems were assumed to have compact spherical configurations. Recent microscopic transport calculations [22,23] indicate however, that multifragment decays may proceed via more complex toroidal or bubble-shaped decay configurations. In this paper, we employ a bond-percolation model to investigate how multifragment disintegrations might be affected by the occurrence of ring- and bubble-shaped decay configurations.

All calculations presented in this paper were performed for a system consisting of $A = N + Z = 250$ nucleons, with $Z = 102$. The decaying system is represented by those points on a simple three-dimensional cubic lattice which fall

within the specified decay volume. Each site represents a nucleon that is "bonded" to its nearest neighbors. Each bond has a uniform probability p to be broken. For each bond a random number is generated between 0 and 1; if this number is smaller than p, the bond is broken, otherwise the bond remains intact. After the status of each bond has thus been determined, connected sites (nucleons) are identified as clusters and assigned their appropriate mass and atomic number. Further details of the model can be found in reference [17].

In the following discussion of non-compact breakup geometries, instrumental distortions will be ignored since we wish to outline some general trends without trying to fit a specific set of data. Nevertheless, it is useful to provide a reference which allows the reader to gauge the magnitude of various effects. For this purpose, the solid points in Figs. 1 and 2 show the fragment admixtures (i.e. the mean number of detected intermediate mass fragments, $\langle N_{IMF} \rangle$, as a function of the detected charged particle multiplicity, N_C) measured [6] for the $^{129}Xe + ^{197}Au$ reaction at E/A = 50 MeV. The solid lines in the figures show previous calculations with the bond percolation model for a compact spherical breakup configuration using a near-critical bond-breaking parameter p = 0.7. These calculations represent the maximum fragment admixtures predicted by the bond-percolation model for a compact spherical geometry; they underpredicted the measured fragment multiplicities [20]. The difference between the thin and thick lines illustrates the magnitude of instrumental distortions. The thin line represents the "raw" calculation (not corrected for the acceptance of the experimental apparatus), and the thick line represents the calculation filtered by the acceptance of the experimental apparatus.

The hatched area in figure 1 shows fragment admixtures predicted for toroidal breakup configurations. In these calculations, the bond breaking probabilities were varied between p = 0.5 - 0.8 and the central radii of the toroids were varied between $R_t = (2.0 - 4.5) \times a$ where $a = \rho_0^{1/3} \approx 1.8$ fm denotes the spacing between adjacent lattice sites (see insert in the figure for a definition of the geometry). Because of volume conservation, the thickness d of the toroid is defined by R_t and the nucleon number: $A \approx \pi^2 R_t d^2/2$. For A=250, the toroid has a hole in the center only for $R_t > 2.5 \times a$. The upper boundary of the hatched area is determined by the breakup of a toroid of radius $R_t = 4.5 \times a$, and the lower boundary represents the breakup of an oblate object of $R_t = 2.0 \times a$. Over the range of $N_C \approx 30 - 50$, the percolation model can produce significantly larger fragment multiplicities for toroidal than for spherical breakup configurations. Qualitatively such an effect may be expected since the surface of a toroid is larger than that of a sphere.

Enhanced fragment admixtures can also be obtained for bubble-shaped breakup configurations, see Fig. 2. The hatched area shows the range of average IMF multiplicities predicted for bond breaking probabilities of p = 0.5 - 0.8 and inner bubble radii of $R_b = (0.0 - 4.0) \times a$ (see insert in the figure for a definition of the geometry). For A = 250 and $R_t > 4.0 \times a$, the bubble has a thickness less than $1.0 \times a$, and the simulation models the breakup of a thin sheet. The upper rising boundary of the hatched area corresponds to calculations with a fixed bond breaking probability of p = 0.5 and varying inner radii, $R_b = (0.0 - 4.0) \times a$. The falling part of the upper boundary represents calculations for an inner radius of $R_b = 4.0 \times a$ and varying bond breaking probabilities p = 0.5 - 0.8. For $\langle N_C \rangle \leq 70$, the lower boundary is given by the breakup of a sphere with varying bond breaking probabilities, p = 0.5 - 0.8.

The results in Figs. 1 and 2 demonstrate that objects with larger surfaces can produce more fragments than objects with smaller surfaces. Hence, geometrical considerations may play an important role for multifragment disintegrations. A relatively cool object (small bond breaking probability) with a large surface may decay into more fragments than a hotter object (larger bond breaking probability) with a smaller surface. For noncompact breakup geometries, the large fragment multiplicities observed for the $^{129}Xe + ^{197}Au$ reaction can be reconciled with predictions of the bond percolation model.

A number of investigations have aimed at obtaining information of near-critical behavior from the shape of fragment mass- or charge-distributions [5,24-27]. Near the critical region, scaling theory of large systems predicts mass distributions of the form:

$$n_A(p) = A^{-\tau} f\left(A^{\sigma}(p - p_c)\right). \qquad (1)$$

Here, τ and σ are critical exponents and $f\left(A^{\sigma}(p - p_c)\right)$ is a scaling function that modulates the power law behavior near the critical bond-breaking probability, $p=p_c$, above which the "infinite" percolation cluster ceases to exist.

In practice, the mass or charge distributions are often fit [24-26] by a simple power law,

$$Y(A) \propto A^{-\lambda}, \qquad (2)$$

where λ is treated as a fit parameter, and the critical exponent τ is identified with the extracted minimum value of λ [15].

We will now show that this empirical approach can lead to misleading results if the geometry at breakup is not compact. For this purpose, we performed power law fits to the mass distributions predicted by the bond percolation model over a broad range of parameters and geometrical

configurations. The results of these calculations are summarized in Figs. 3 and 4 for toroidal and bubble-shaped geometries, respectively. In both cases, the best fit-parameter λ exhibits a clear valley as a function the bond-breaking (p) and geometry (R_t and R_b) parameters. In this valley, smaller values of λ occur for less compact breakup geometries.

The strong geometry-dependence of the relation between the power-law exponent λ and the bond-breaking parameter p is depicted more clearly in Fig. 5 for three representative breakup configurations, a solid sphere (solid circles), a toroid of central radius $R_t = 3.0 \times a$ (open diamonds), and a bubble with inner radius $R_b = 3.0 \times a$ (solid squares).

Microscopic transport calculations [22,23] predict a strong dependence of the breakup geometry upon beam energy, impact parameter, and projectile-target combination. Indeed, under favorable conditions, the formation of unstable bubbles and rings has been predicted [22,23]. The present model calculations for finite systems indicate a strong dependence of extracted "critical" parameters (τ and p_c) on the geometrical configuration of the system at breakup. Compilations of power law exponents λ determined from data for different entrance channels [24], for different impact parameters [26], or for excitation functions covering broad ranges of energies [24,25,27] may contain samples representing sufficiently different geometrical configurations to render a minimum in λ difficult to interpret. For infinite systems, critical exponents govern the scaling laws near critical points. We suspect that the application of scaling laws to finite systems of potentially complex breakup geometries is much less straight forward than originally surmised [28].

In conclusion, we have explored the multifragment breakup of different geometrical configurations by means of a simple bond-percolation model. Our

calculations indicate enhanced fragment production from systems with larger surfaces and a strong geometry-dependence of the power-law exponents which characterize the shapes of mass distributions. Of course, the existence of such non-compact breakup configurations is not yet established. This question still remains to be answered.

This work was supported by the National Science Foundation under Grant No. PHY-9214992.

References

1. G. Bertsch and P.J. Siemens, Phys. Lett. **B126** (1983) 9.
2. A.S. Hirsch et al., Phys. Rev. **C29** (1984) 508.
3. L.P. Cernai and J. Kapusta, Phys. Rep. **131** (1986) 223.
4. W.G. Lynch, Ann. Rev. Nucl. Sci. **37** (1987) 493.
5. D.H. Gross, Rep. Prog. Phys. **53** (1990) 605.
6. D.R. Bowman et al., Phys. Rev. Lett. **67** (1991) 1527.
7. R.T. de Souza et al., Phys. Lett. **B268** (1991) 6.
8. K. Hagel et al., Phys. Rev. Lett. **68** (1992) 2141.
9. L.G. Moretto, Nucl. Phys. **A247** (1975) 211.
10. J. Randrup and S. E. Koonin, Nucl. Phys. A **356** (1981) 223.
11. J. P. Bondorf, Nucl. Phys. **A387** (1982) 25c.
12. W.A. Friedman and W.G. Lynch, Phys. Rev. **C28** (1982) 16.
13. W.A. Friedman, Phys. Rev. Lett. **60** (1988) 2125.
14. W.A. Friedman, Phys. Rev. **C42** (1990) 667.
15. W. Bauer et al., Phys. Lett. **150B** (1985) 53.
16. W. Bauer, U. Post, D.R. Dean and U. Mosel, Nucl. Phys. **A452** (1986) 699.
17. W. Bauer, Phys. Rev. **C38** (1988) 1297.
18. X. Campi, Phys. Lett. **B208** (1988) 351.
19. C. Ngô et al., Nucl. Phys. **A499** (1989) 148.
20. L. Phair et al., Phys. Lett. **B285** (1992) 10.
21. L. Phair et al., Phys. Lett. **B291** (1992) 7.
22. W. Bauer, G.F. Bertsch and H. Schulz, Phys. Rev. Lett. **69** (1992) 1888.
23. L.G. Moretto et al., Phys. Rev. Lett. **69** (1992) 1884.
24. A.D. Panagiotou et al., Phys. Rev. Lett. **52** (1984) 496.
25. M. Mahi et al., Phys. Rev. Lett. **60** (1988) 1936.
26. C.A. Ogilvie et al., Phys. Rev. Lett. **67** (1991) 1214.
27. T. Li et al., Phys. Rev. Lett. **70** (1993) 1924.
28. X. Campi and H. Krivine, Z. Phys. **A344** (1992) 81.

Figure Captions:

Fig. 1: Relation between average IMF and charged particle multiplicities. Solid points represent values measured for $^{129}Xe + ^{197}Au$ at E/A=50 MeV. Thin (thick) solid line shows the raw (efficiency corrected) percolation calculation for a solid sphere. The hatched area shows the range of average IMF and *average* charged particle multiplicities predicted by percolation calculations for toroidal breakup configurations.

Fig. 2: Relation between average IMF and charged particle multiplicities. Solid points represent values measured for $^{129}Xe + ^{197}Au$ at E/A=50 MeV. Thin (thick) solid line shows the raw (efficiency corrected) percolation calculation for a solid sphere. The hatched area shows the range of average IMF and *average* charged particle multiplicities predicted by percolation calculations for bubble-shaped breakup configurations.

Fig. 3: Extracted power-law exponents λ fit to mass distributions predicted by the bond percolation model for the break up of toroidal systems as a function of R_t and p.

Fig. 4: Extracted power-law exponents λ fit to mass distributions predicted by the bond percolation model for the break up of bubble shaped systems as a function of R_b and p.

Fig. 5: λ as function of p for a solid sphere (circles), a toroid of radius $R_t = 3.0 \times a$ (diamonds), and bubble with inner radius $R_b = 3.0 \times a$ (squares).

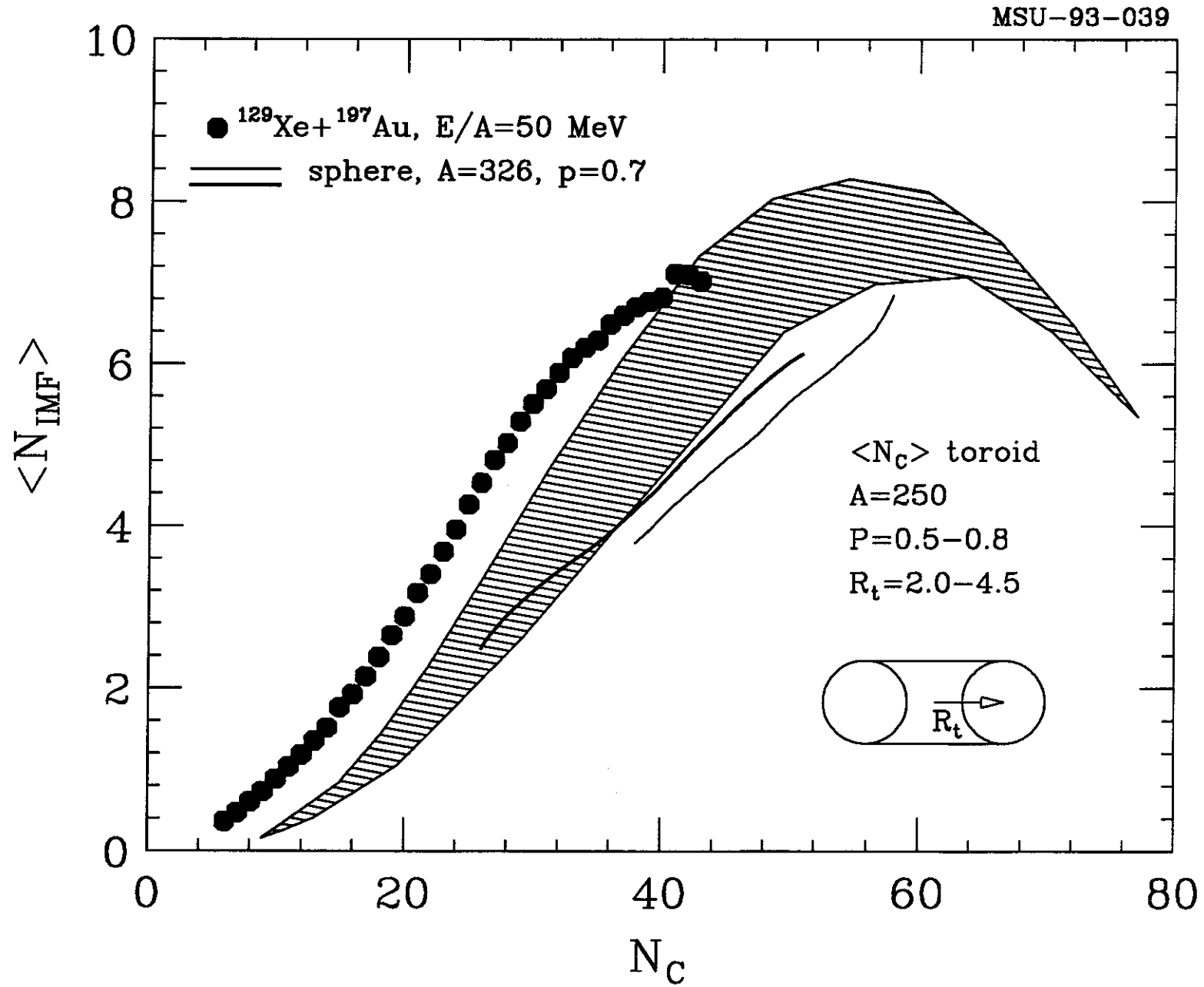
MSU-93-039
^{129}Xe+^{197}Au, E/A=50 MeV
sphere, A=326, p=0.7
<N$_c$> toroid
A=250
P=0.5–0.8
R$_t$=2.0–4.5
R$_t$
<N$_{IMF}$>
N$_c$
0
2
4
6
8
10
0
20
40
60
80

Fig. 1

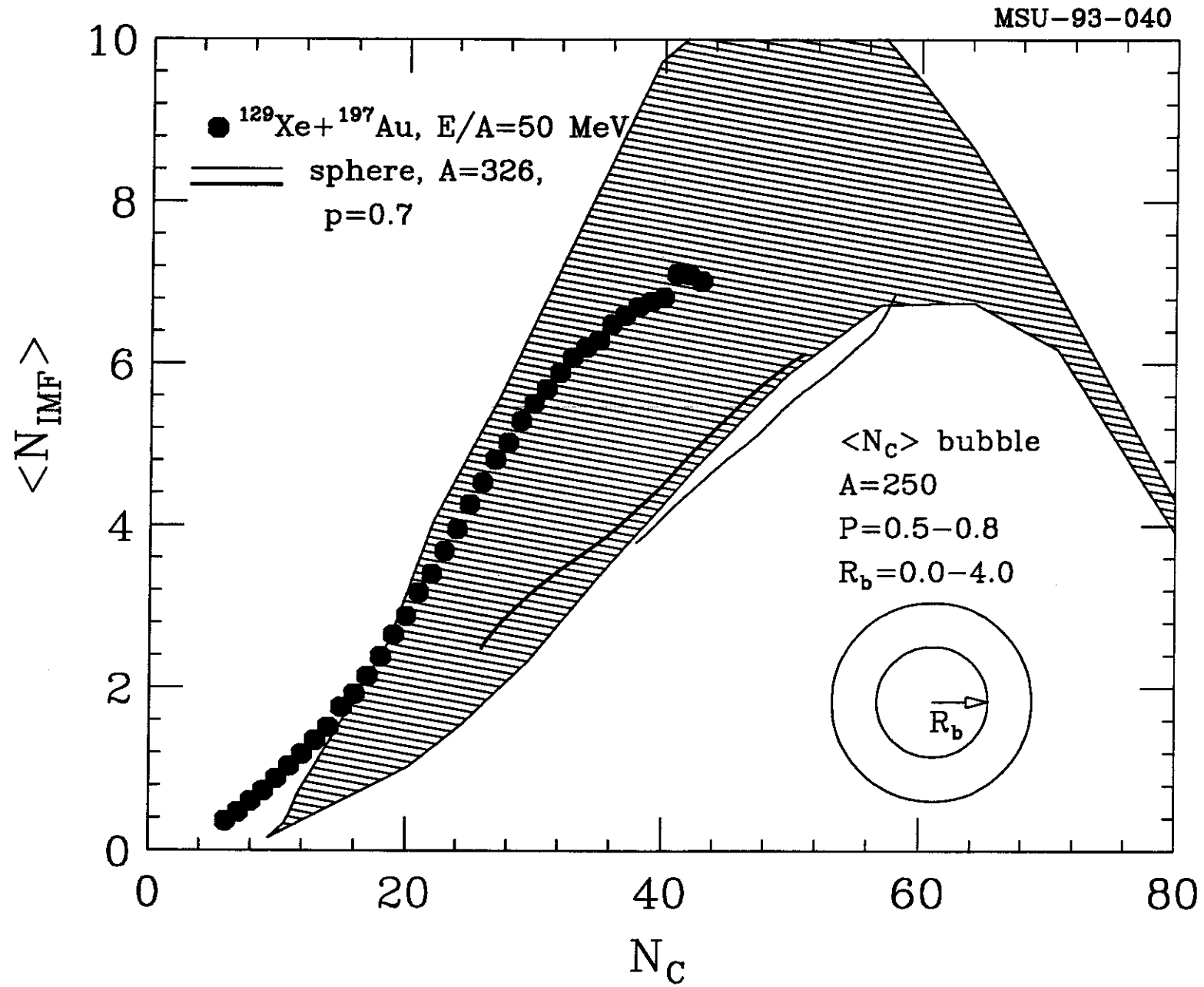
MSU-93-040
$^{129}Xe+^{197}Au$, E/A=50 MeV
sphere, A=326,
p=0.7
<N_c> bubble
A=250
P=0.5-0.8
R_b=0.0-4.0
R_b
<N_{IMF}>
N_c
0
2
4
6
8
10
0
20
40
60
80

Fig. 2

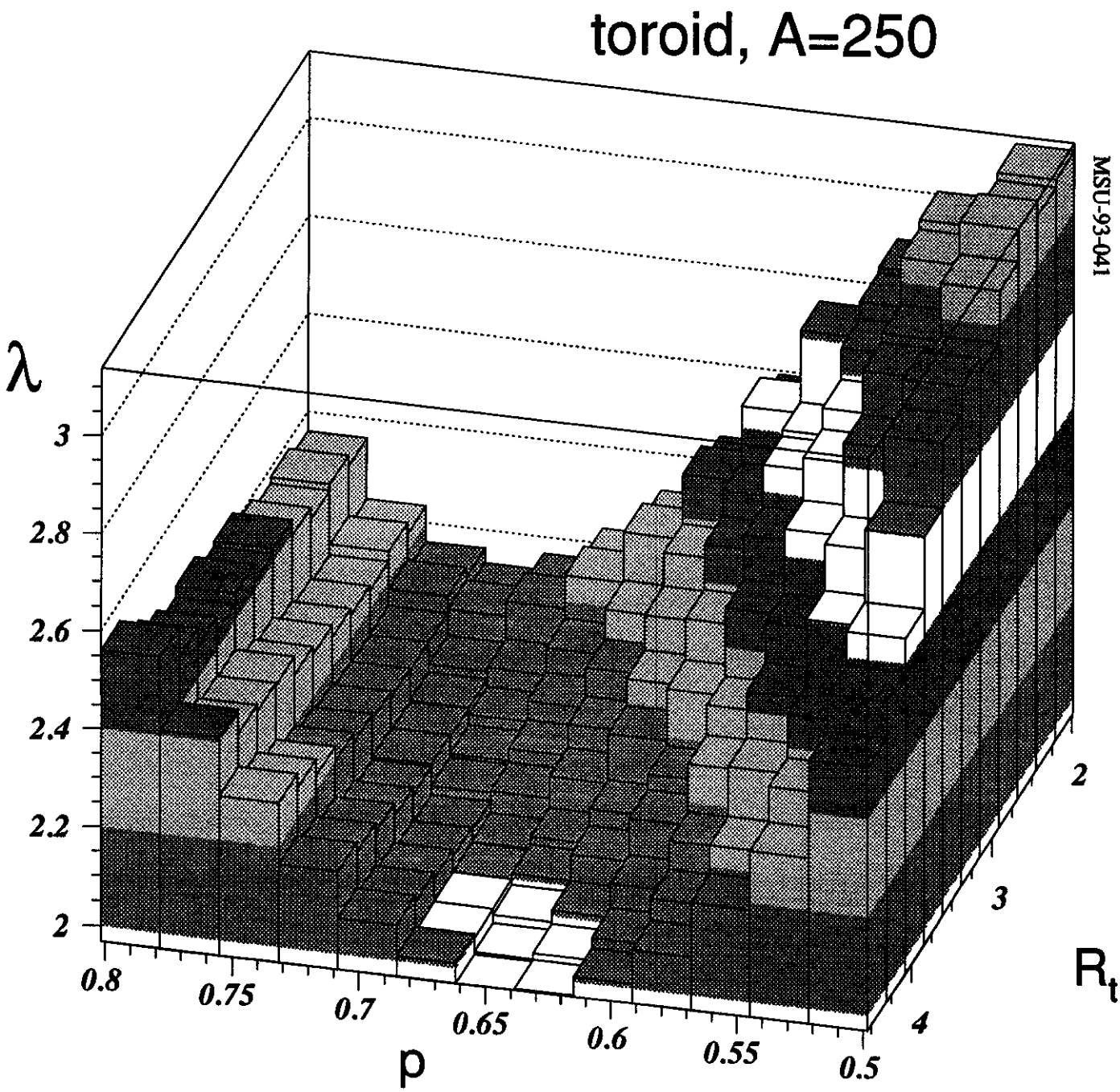
toroid, A=250
MSU-93-041
λ
3
2.8
2.6
2.4
2.2
2
0.8
0.75
0.7
0.65
0.6
0.55
0.5
p
2
3
4
R_t

Fig.3

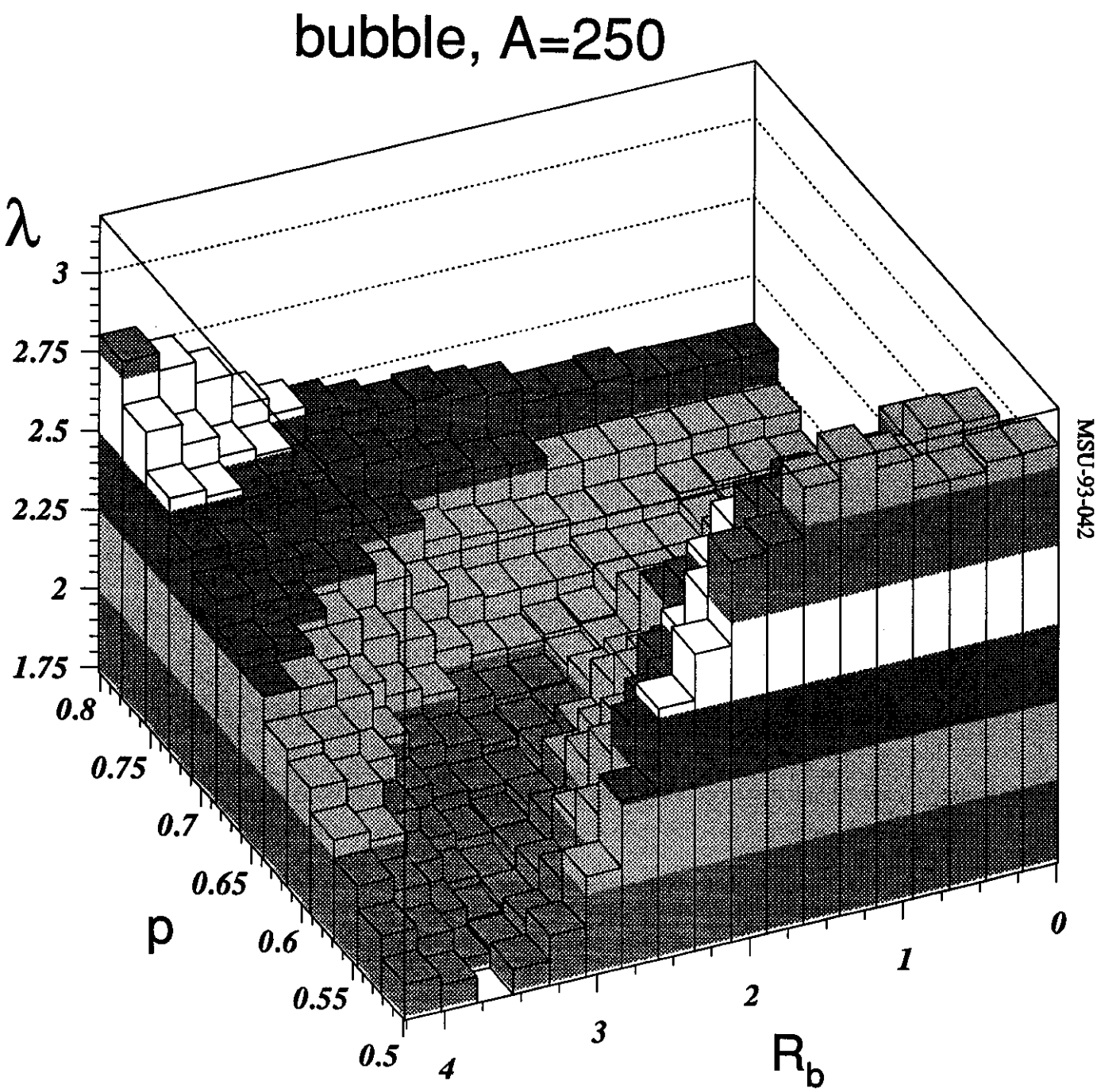
bubble, A=250
λ
3
2.75
2.5
2.25
2
1.75
0.8
0.75
0.7
0.65
0.6
0.55
0.5
p
4
3
2
1
0
R_b
MSU-93-042

Fig. 4

Fig 5

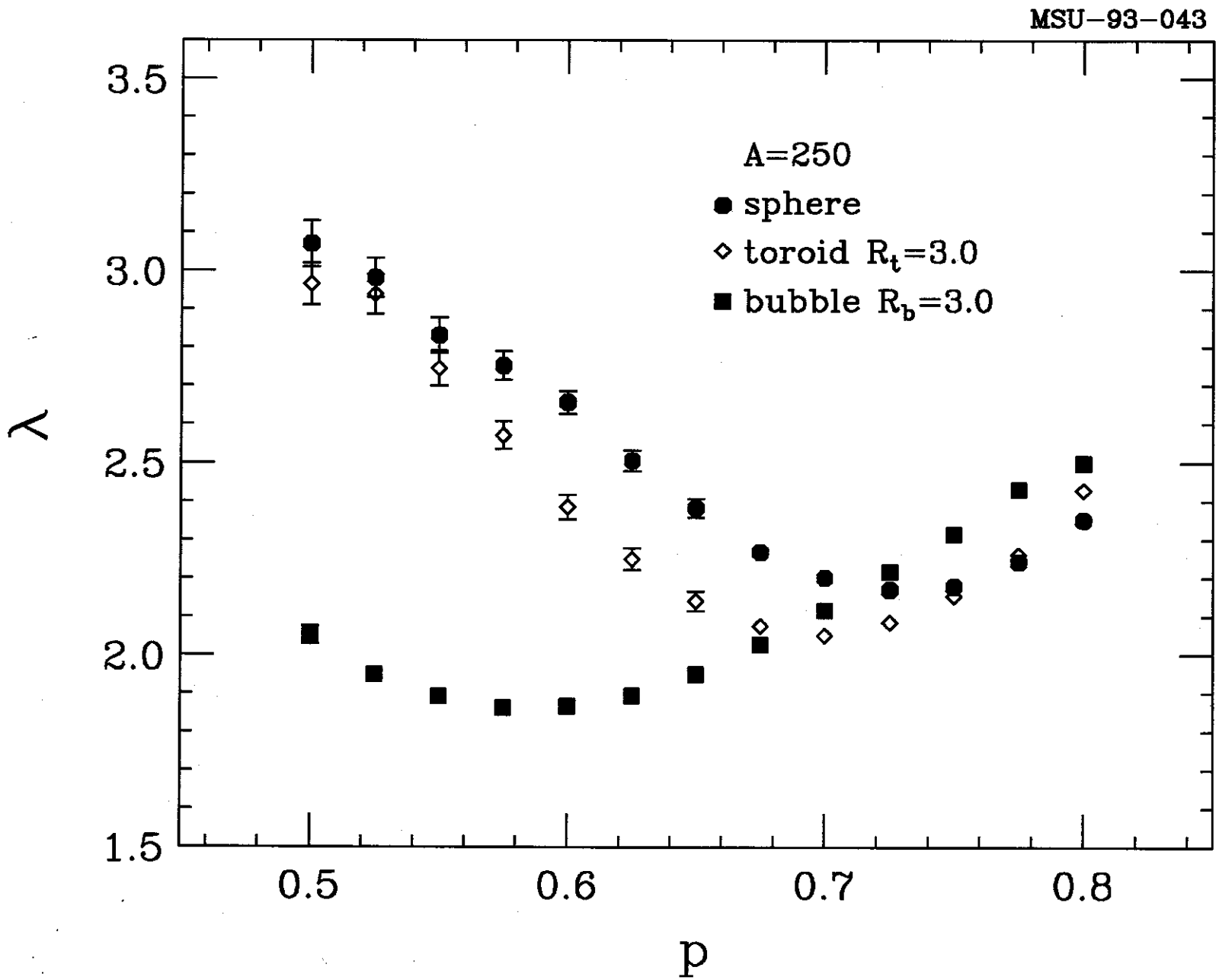
MSU-93-043
A=250
sphere
toroid R_t=3.0
bubble R_b=3.0
λ
p
3.5
3.0
2.5
2.0
1.5
0.5
0.6
0.7
0.8